

A Three-Layer Alternating Spinning Circulation in the South China Sea

JIANPING GAN, ZHIQIANG LIU, AND CHIWING REX HUI

Department of Mathematics and Division of Environment, Hong Kong University of Science and Technology, Hong Kong, China

(Manuscript received 23 February 2016, in final form 14 April 2016)

ABSTRACT

Understanding of the three-dimensional circulation in the South China Sea (SCS) is crucial for determining the transports of water masses, energy, and biogeochemical substances in the regional and adjacent larger oceans. The circulation's kinematic and dynamic natures, however, are largely unclear. Results from a three-dimensional numerical ocean circulation model and geostrophic currents, derived from hydrographic data, reveal the existence of a unique, three-layer, cyclonic–anticyclonic–cyclonic (CAC) circulation in the upper (<750 m), middle (750–1500 m), and deep (>1500 m) layers in the SCS with differing seasonality. An inflow–outflow–inflow structure in Luzon Strait largely induces the CAC circulation, which leads to vortex stretching in the SCS basin because of a lateral planetary vorticity flux in each of the respective layers. The formation of joint effects of baroclinicity and relief (JEBAR) is an intrinsic dynamic response to the CAC circulation. The JEBAR arises from the CAC flow–topography interaction in the SCS.

1. Introduction

The South China Sea (SCS) has a deep, central basin surrounded by a steep continental slope and links to the western Pacific Ocean via Luzon Strait, to the Java Sea via Karimata Strait, to the East China Sea via Taiwan Strait, and to the Sulu Sea via Mindoro Strait (Fig. 1).

The East Asia monsoonal winds, and lateral inflow/outflow through the straits around the periphery of the SCS, jointly force the seasonal circulation pattern in the SCS basin (Qu 2000). During winter, the northeasterly monsoonal winds have a dominant positive wind stress curl in the deep basin. The winds turn southwesterly with a much weaker positive wind stress curl during summer. An annual-mean westward transport of $\sim 4\text{--}10\text{ Sv}$ ($1\text{ Sv} \equiv 10^6\text{ m}^3\text{ s}^{-1}$) from the Pacific to the SCS through Luzon Strait has been widely reported in previous studies (e.g., Wyrski 1961; Chen and Huang 1996; Qu et al. 2000, 2004; Xue et al. 2004; Tian et al. 2006). Based on these studies, a sandwichlike inflow–outflow–inflow pattern in

the upper, middle, and deep layers of Luzon Strait, respectively, has been identified, though the depth ranges of the three layers are different from different studies. The intrusive transport through Luzon Strait is balanced by the extrusive transport through all other straits in the upper layer and through Luzon Strait in the middle layer. As a result of both wind and lateral forcing, the basin circulation in the upper layer of the SCS is cyclonic in winter, and, in summer, it is cyclonic in the northern half of the basin and anticyclonic in the southern half of the basin (Qu 2000). In the deep layer, there is a cyclonic circulation (Wang et al. 2011; Lan et al. 2013).

However, we still do not understand the overall vertical structure of circulation and its seasonality, especially regarding the dynamic coherence of the circulation in the water column in the SCS. We also have little knowledge of the relative importance of the wind forcing, lateral inflow/outflow, and intrinsic dynamics that arise from the flow–topography interaction on the SCS circulation. Filling this knowledge gap will provide insight into the basin circulation physics in the SCS and other oceans that are driven by multiforcing processes.

2. Materials and methods

a. Ocean model

We use the Regional Ocean Modeling System (ROMS; Shchepetkin and McWilliams 2005) to

 Denotes Open Access content.

Corresponding author address: Jianping Gan, Department of Mathematics, Hong Kong University of Science and Technology, Clear Water Bay, Kowloon, Hong Kong, China.
E-mail: magan@ust.hk

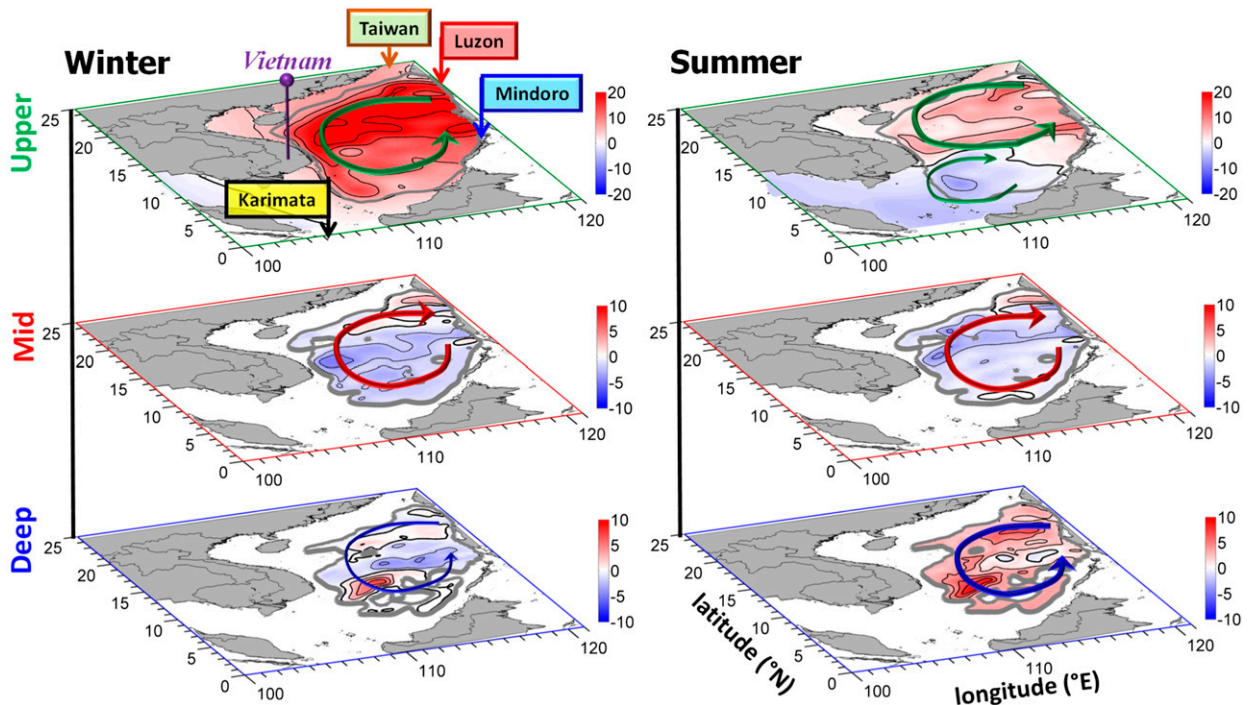


FIG. 1. Simulated transport streamfunctions (Sv) in the upper (<750 m), middle (mid) (750 – 1500 m), and deep layers (>1500 m) in (left) winter and (right) summer in the South China Sea. The circles represent the mean circulation in each layer. The thick contour line in the upper layer refers to the edge of the basin along the 100-m isobath. A thinner circular line in the schematic circulation represents a relatively weak circulation.

simulate three-dimensional, time-dependent circulation. The model domain covers all the China seas (SCS, East China Sea, Yellow Sea, and Bohai Sea) from $\sim 0^\circ$ to $\sim 49^\circ N$ and extends to the central Pacific Ocean. We adopt a curvilinear grid with ~ 10 -km horizontal grid size and a 30-level stretched generalized terrain-following vertical coordinate.

We force the model with climatological (averaged from 1981 to 2010) wind stress calculated from monthly reanalysis of blended sea winds ($0.25^\circ \times 0.25^\circ$) at 10 m released from the National Oceanic and Atmospheric Administration (NOAA; <https://www.ncdc.noaa.gov/oa/rsad/air-sea/seawinds.html>), using the bulk formulation by Large and Pond (1981). We calculate the atmospheric heat and salt fluxes from climatological-mean monthly National Centers for Environmental Prediction (NCEP) Reanalysis-1 meteorological variables. The reanalysis has $\sim 1.875^\circ$ resolution.

We apply active open boundary conditions (OBCs) to integrate external tidal and subtidal forces along the open boundaries of the computational domain. The OBCs are similar to Gan and Allen (2005). The external forcing of velocities and thermohaline variables along the boundaries are provided by the climatological monthly solutions of the Ocean General

Circulation Model For the Earth Simulator (OFES) global model (Sasaki et al. 2008) and by tidal forcing using eight harmonic constituents (M_2 , S_2 , N_2 , K_2 , K_1 , O_1 , P_1 , and Q_1) from the Inverse Tide Model (ITM; Egbert et al. 1994). To account for the self-attraction and loading effect of the ocean, we add tidal potential to the pressure term following Ray (1998). We initialize the model with winter climatological *World Ocean Atlas 2013* (Locarnini et al. 2013; Zweng et al. 2013) potential temperature and salinity and spun up the model for 50 yr. We use the last 5-yr-averaged values of the model's output variables for the analyses in this study.

Our circulation model is part of the China Sea Multi-Scale Ocean Modeling System (CMOMS) that integrates coupled physical–biogeochemical processes in estuary/shelf/basin/open oceans within different subscales in the China Seas. CMOMS has been extensively validated by measurements and physics (Gan et al. 2016, manuscript submitted to *J. Geophys. Res.*).

b. Hydrographic data and geostrophic currents

We use monthly averaged hydrographic data to calculate the geostrophic velocity in the water column

based on the thermal wind relation. The data are from the U.S Navy Generalized Digital Environment Model (GDEM, version 3.0), which is gridded ocean temperature and salinity (T - S) data generated by 4.5-million observed T - S profiles dating back to 1920 (Carnes 2009). The GDEM data have a horizontal resolution of $0.25^\circ \times 0.25^\circ$ and a vertical resolution that ranges from 2 m in the upper 1600 m to 200 m from 1600 to 6600 m. We use 500 m (Qu et al. 2000) and 2400 m (Wang et al. 2011) as the levels of no motion to derive the geostrophic currents in the upper 1500 m and below 1500 m. These reference depths appear to be reasonable according to the three-layer circulation shown in this study.

3. Three-layer basin circulation

a. Three-layer basin circulation

Figure 1 displays the three-layer circulation in the model results for the SCS. The circulation is represented by the seasonal layer-integrated transport streamfunction ψ in the upper (<750 m), middle (750–1500 m), and deep (>1500 m) layers. The seasonal variation of the circulation Γ can be further depicted by the time series of the domain-averaged vorticity in the water column. According to Stokes' theorem,

$$\Gamma = \oint \mathbf{V} \cdot d\mathbf{l} = \iint \zeta \cdot d\mathbf{A}, \quad (1)$$

where \mathbf{V} is the velocity vector, and ζ is the relative vertical vorticity normal to A , the area of a specific sea where water depth is $h > 100$ m. We estimate the thickness of these three layers from the vertical profiles of the domain-averaged vorticity shown in Fig. 2a.

In the upper layer, a basinwide cyclonic circulation characterizes the SCS circulation in winter. The cyclonic circulation is stronger in the northern half of the basin. The circulation pattern is the result of forcing by the northeasterly monsoon wind stress, positive wind stress curl, and a stronger winter Kuroshio intrusion along the continental slope around the SCS (e.g., Qu 2000; Gan et al. 2006). However, in summer, a southwestward current along the northern slope and an eastward returning current at $\sim 13^\circ\text{N}$ form a cyclonic circulation in the northern half of the basin and a weak anticyclonic circulation in the southern part of the basin. The cyclonic and anticyclonic circulations are separated by the $\psi = 0$ contour line (Fig. 1) associated with the zero wind stress curl line in the dipole wind stress curl and with the recirculation in a coastal jet separation to the east of Vietnam (Gan and Qu 2008).

Unlike the flow pattern in the upper layer, the circulation in the middle layer of the SCS is distinctly

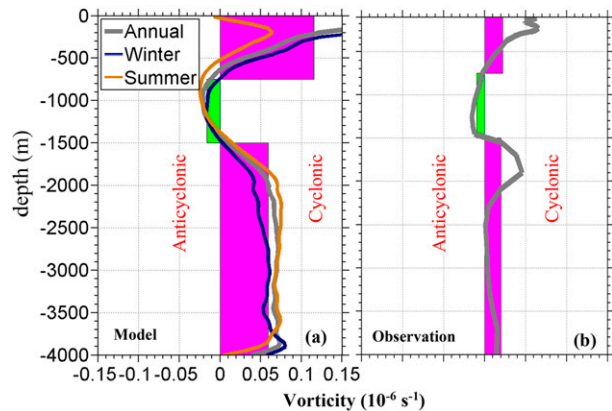


FIG. 2. Domain-averaged annual- and seasonal-mean vorticity as a function of depth from (a) model results and (b) annual-mean geostrophic current velocities derived from GDEM hydrographic data. Green (negative) and purple (positive) bars are the averaged vorticity in the specific layers.

characterized by an anticyclonic circulation during winter and summer, and the circulation is more intense in summer.

In the deep layer, the SCS is dominated by a cyclonic circulation in both winter and summer, as was also observed by Wang et al. (2011) and Lan et al. (2013). Similar to what occurs in the middle layer, the intensity of the cyclonic circulation in the deep layer is stronger in summer than in winter, opposite to what occurs in the upper layer.

Similar to what ψ illustrates in Fig. 1, Γ exhibits a clear three-layer alternating cyclonic–anticyclonic–cyclonic (CAC) circulation in the upper–middle–deep layers of the water column (Fig. 2a). The data-derived geostrophic currents also show the existence of the CAC circulation (Fig. 2b).

b. Lateral transports in the SCS basin

The three-layer CAC circulation in the SCS has a coherent link with the similar sandwichlike inflow–outflow–inflow in Luzon Strait (Fig. 3a). Meanwhile, the outflows through Mindoro Strait (Fig. 3b) and crossing the 100-m isobath (Fig. 3c) provide the necessary mass balance in the basin. The sandwichlike vertical structure of the inward–outward–inward transport through Luzon Strait has annual-mean, layer-integrated transports of ~ -5.9 , ~ 1.4 , and ~ -0.9 Sv in the upper, middle, and deep layers, respectively. Our net transport of -5.4 Sv is similar to those derived from observations by Chu and Li (2000), Su (2004), and Tian et al. (2006). The mean transport in the each of the three layers varied greatly among different measurements, which ranged from -10 to -3.5 , 5 to 0.22 , and -2 to -0.22 Sv in the upper, middle, and deep layers (e.g., Tian et al. 2006; Yuan et al. 2008), respectively. Our deep inward transport of -0.9 is smaller than ~ -1.5 Sv derived

from a short-term observation by Zhao et al. (2014), who attributed the formation of the deep inflow to a baroclinic pressure gradient across Luzon Strait. The intrusive transport from Luzon Strait is balanced by the outward transports of ~ 3.2 Sv through Mindoro Strait and of ~ 2.3 Sv crossing the 100-m isobath (Figs. 3b,c). The transport of Mindoro Strait is similar to the finding of Qu and Song (2009), and the transport crossing the 100-m isobath equals the sum of the transports in Taiwan Strait (1.2 Sv) and Karimata Strait (1.1 Sv).

Strong seasonality also exists in these lateral transports, similar to CAC circulation. The weakened Kuroshio in winter is favorable to the upper-layer intrusion in Luzon Strait (Qu et al. 2000), and the net westward transport in Luzon Strait strengthens from

summer to winter (Fig. 3a). As a result, the outward transports through Mindoro Strait and crossing the 100-m isobath are stronger in winter (Figs. 3b,c). The transport crossing the 100-m isobath has an opposite phase between winter and summer and between the upper and lower layer.

c. Vorticity dynamics of the CAC circulation

To identify the multiforcing processes of winds, lateral fluxes, and intrinsic dynamics of flow–topography interaction, we use a domain-integrated vorticity balance in each of the layers to identify the source of forcing to the CAC circulation. We present the domain- and layer-integrated vorticity Ω equation as

$$\begin{aligned} \int_A \overline{\Omega}_t dA = & \underbrace{-\int_A [(f\bar{u}D)_x + (f\bar{v}D)_y] dA}_{\Omega^{\text{cor}}} - \underbrace{\int_A \nabla_H \times (\text{HNL}) dA}_{\Omega^{\text{adv}}} + \underbrace{\int_A \nabla \times \int_{Lb}^{Lu} \text{hvisc} dz dA}_{\Omega^{\text{hadv}}} - \underbrace{\int_A \nabla_H \times (\text{VNL}) dA}_{\Omega^{\text{vadv}}} \\ & + \underbrace{\int_A \frac{1}{\rho_o} [J(Lb, P^{Lb}) + J(Lu, P^{Lu})] dA}_{\Omega^{\text{pgf}}} + \underbrace{\int_A \nabla_H \times \int_{Lb}^{Lu} [K_v(\bar{\mathbf{V}})_z]_z dz dA}_{\Omega^{\text{vis}}}; \end{aligned} \quad (2)$$

$$\text{for the upper layer, } Lu = \eta \quad \text{and} \quad Lb = \begin{cases} h(x, y), & -750 < h < -100 \text{ m}; \\ -750 \text{ m}, & h \geq -750 \text{ m} \end{cases};$$

$$\text{for the middle layer, } Lu = -750 \text{ m} \quad \text{and} \quad Lb = \begin{cases} h(x, y), & -1500 < h < -750 \text{ m}; \\ -1500 \text{ m}, & h \geq -1500 \text{ m} \end{cases}; \quad \text{and}$$

$$\text{for the deep layer, } Lu = -1500 \text{ m} \quad \text{and} \quad Lb = h(x, y).$$

The terms Lu and Lb are the depths of the top and bottom for each specific layer, respectively; η is sea level and $D = Lu - Lb$; u and v are the zonal (x) and meridional (y) velocities, respectively; f is the Coriolis parameter; HNL is the horizontal nonlinear advection plus horizontal viscous term (hvisc); the horizontal viscous term is generally very small; VNL is the vertical advection term; K_v is the vertical viscous coefficient; P^{Lu} and P^{Lb} are pressure at the top and bottom of each layer, respectively; and J is a Jacobean operator. The overbar refers to the layer average and the suffix represents derivation.

The terms in Eq. (2), from the left to right, are acceleration Ω^{acce} , divergence Ω^{cor} (vortex stretching), horizontal advection Ω^{hadv} , tilting Ω^{vadv} , pressure curl Ω^{pgf} , and vertical viscosity Ω^{vis} . The Ω^{vis} can be expressed as $\Omega^{\text{vis}} = \Omega^{\text{sstr}}$ (wind stress curl) $- \Omega^{\text{bstr}}$ (bottom stress curl) in the upper layer. The tilting of

horizontally oriented components of vorticity into the vertical by a nonuniform vertical velocity field generates the tilting term Ω^{vadv} . The Ω^{pgf} , or joint effect of baroclinicity and relief (JEBAR), is generated by a pressure torque that is formed by the interaction between baroclinically induced pressure and the variable slope topography (Mertz and Wright 1992). Figure 4 shows the balance of Eq. (2) in the each of the three layers.

In the upper layer, in winter, Ω^{cor} and Ω^{sstr} are the major sources of the cyclonic circulation. The two terms are mainly balanced by JEBAR and Ω^{bstr} . In summer, the main source for the relatively weak cyclonic circulation becomes Ω^{hadv} and Ω^{cor} , while Ω^{sstr} has a very small influence. The summer source terms are also balanced mainly by JEBAR. In both winter and summer, Ω^{acce} is negative, which suggests that the cyclonic circulation weakens following the autumn and spring accelerations.

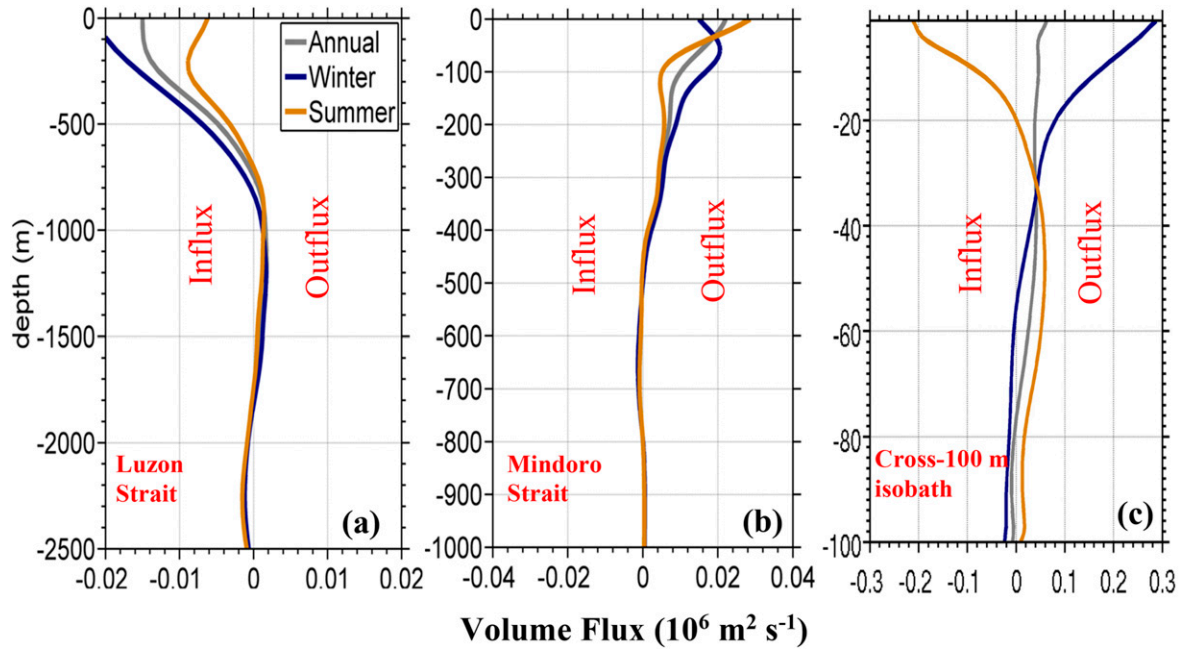


FIG. 3. Simulated volume flux as a function of depth normal to (a) Luzon Strait, (b) Mindoro Strait, and (c) the 100-m isobath, respectively.

In the middle and deep layers, Ω^{cor} is also the main source term for the respective anticyclonic and cyclonic circulation. It balances primarily the JEBAR and secondarily other relatively small terms. The signs for

almost all terms in the middle layer are the opposite those of the upper and deep layers. The magnitudes of all the terms and their seasonality are much smaller in middle and lower layers than in the upper layer.

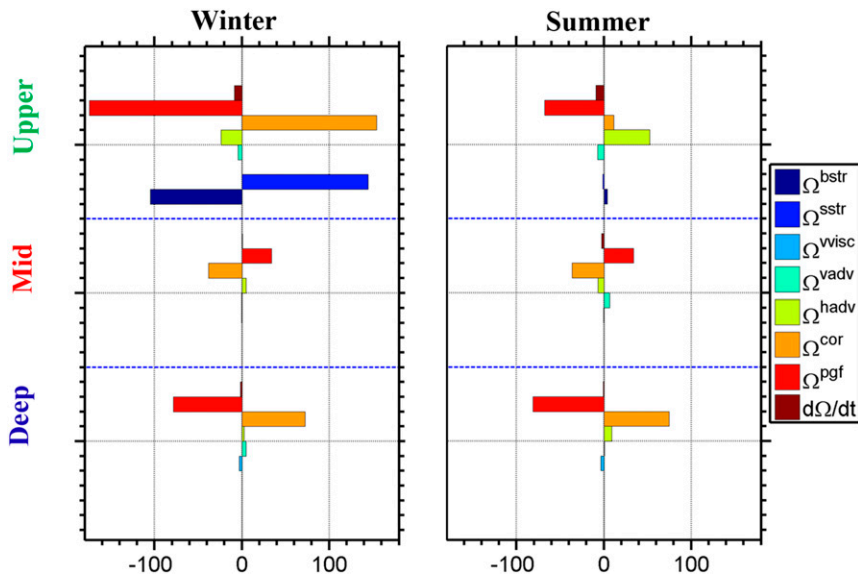


FIG. 4. Terms ($m^3 s^{-2}$) of domain and layer-integrated vorticity equation in the upper, middle (mid), and deep layers during (left) winter and (right) summer: Ω^{acce} is acceleration, Ω^{cor} is divergence or vortex stretching, Ω^{hadv} is horizontal advection, Ω^{vadv} is tilting, Ω^{pgf} is the pressure curl, Ω^{vis} is vertical viscosity (middle and deep layers), Ω^{sstr} is wind stress curl, and Ω^{bstr} is bottom stress curl in the upper layer.

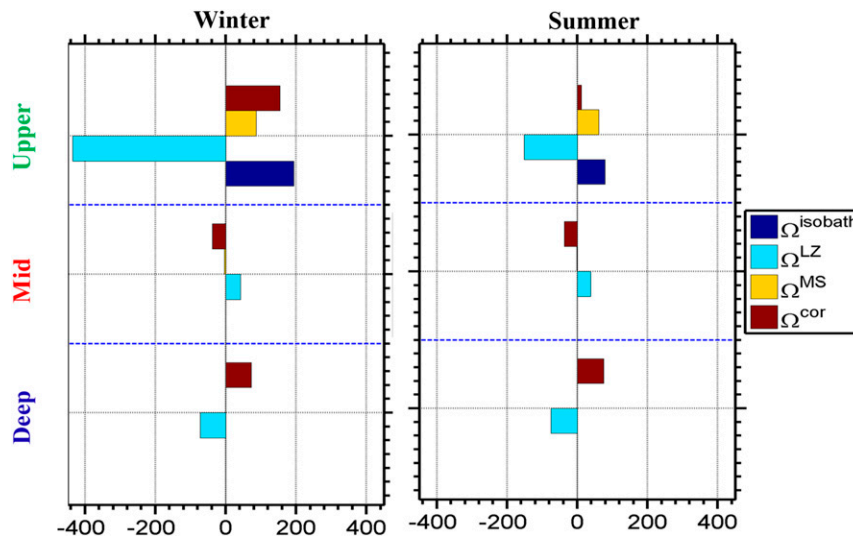


FIG. 5. Mean values of Ω^{cor} term ($\text{m}^3 \text{s}^{-2}$) in the upper, middle (mid), and deep layers and the respective contributions by planetary vorticity flux through Luzon Strait Ω^{LZ} , Mindoro Strait Ω^{MS} , and crossing the 100-m isobath Ω^{isobath} in winter and summer.

Thus, Ω^{cor} is the dominant vorticity source in each layer of the CAC circulation. Meanwhile, JEBAR acts as the primary response to the CAC circulation in the SCS basin. We use a divergence theorem to relate the forcing mechanism of the CAC circulation to the flux that crosses the meridionally oriented section Si along Luzon Strait and both the meridionally (Si) and zonally oriented (Sj) sections along Mindoro Strait and along the 100-m isobath. The Si and Sj are positive outward of the enclosed SCS area. We express the dominant vorticity source Ω^{cor} as

$$\Omega^{\text{cor}} = - \int_{Si} f \bar{u} dSi - \int_{Sj} f \bar{v} dSj. \quad (3)$$

All terms in Eq. (3) are represented by the values on the left side of the equation in Fig. 5.

The planetary vorticity flux through Luzon Strait Ω^{LZ} primarily contributes to Ω^{cor} in all the layers during winter and summer (Fig. 5). The vertical structure of Ω^{LZ} has alternating negative–positive–negative signs in the upper–middle–deep layers that correspond to the sandwichlike structure of the volume flux in Luzon Strait (Fig. 3a). The seasonal variation of Ω^{LZ} is also well-correlated with the seasonal variation of the volume flux in Luzon Strait. The inputs of the planetary vorticity flux in the upper and deep layers from Luzon Strait are offset by the outputs of the fluxes crossing the isobath and through Mindoro Strait. The cross-isobath flux transports Ω^{cor} toward the shallower shelf waters, and most of it will exit the SCS through the Taiwan Strait and Karimata Strait. The contribution

from Mindoro Strait Ω^{MS} is relatively small as compared with that from Ω^{LZ} , particularly in winter.

4. Summary

Using observations and results from a numerical model, we identify a new CAC circulation pattern in the SCS. We attribute the CAC circulation to vortex stretching from the planetary vorticity flux that is extrinsically induced by the inflow–outflow–inflow in the upper–middle–deep layers through Luzon Strait. We also attribute the cyclonic circulation in the upper layer to wind stress curl in winter and nonlinear advection in summer. The inflow–outflow–inflow in Luzon Strait interacts with the interior circulation of the SCS, and it varies coherently with the overall CAC circulation. JEBAR, related to bottom pressure torque, forms in each specific layer as a result of interaction between the CAC flow and bottom topography. Vortex stretching is predominantly balanced by the JEBAR. The planetary vorticity outfluxes that cross the edge of the basin and the Mindoro Strait offset the influx from Luzon Strait. These outfluxes around the SCS, together with the influx from Luzon Strait, are necessary in sustaining the CAC circulation.

Acknowledgments. This research was supported by the National (China) Key Basic Research Development Program (2015CB954004), the Key Project of the National Science Foundation of China (91228202 and 91328202), and Hong Kong Research Grant Council (GRF16202514).

REFERENCES

- Carnes, M. R., 2009: Description and evaluation of GDEM-V 3.0. Naval Research Laboratory Rep. NRL/MR/7330-09-9165, 21 pp.
- Chen, C.-T. A., and M. H. Huang, 1996: A mid-depth front separating the South China Sea water and the Philippine Sea water. *J. Oceanogr.*, **52**, 17–25, doi:10.1007/BF02236530.
- Chu, P. C., and R. Li, 2000: South China Sea isopycnal-surface circulation. *J. Phys. Oceanogr.*, **30**, 2419–2438, doi:10.1175/1520-0485(2000)030<2419:SCSISC>2.0.CO;2.
- Egbert, G. D., A. F. Bennett, and M. G. G. Foreman, 1994: TOPEX/Poseidon tides estimated using a global inverse model. *J. Geophys. Res.*, **99**, 24 821–24 852, doi:10.1029/94JC01894.
- Gan, J., and J. S. Allen, 2005: On open boundary conditions for a limited-area coastal model off Oregon. Part 1: Response to idealized wind forcing. *Ocean Modell.*, **8**, 115–133, doi:10.1016/j.ocemod.2003.12.006.
- , and T. Qu, 2008: Coastal jet separation and associated flow variability in the southwest South China Sea. *Deep-Sea Res. I*, **55**, 1–19, doi:10.1016/j.dsr.2007.09.008.
- , H. Li, E. N. Curchitser, and D. B. Haidvogel, 2006: Modeling South China Sea circulation: Response to seasonal forcing regimes. *J. Geophys. Res.*, **111**, C06034, doi:10.1029/2005JC003298.
- Lan, J., N. Zhang, and Y. Wang, 2013: On the dynamics of the South China Sea deep circulation. *J. Geophys. Res. Oceans*, **118**, 1206–1210, doi:10.1002/jgrc.20104.
- Large, W. G., and S. Pond, 1981: Open ocean momentum flux measurements in moderate to strong winds. *J. Phys. Oceanogr.*, **11**, 324–336, doi:10.1175/1520-0485(1981)011<0324:OOMFMI>2.0.CO;2.
- Locarnini, R. A., and Coauthors, 2013: *Temperature*. Vol. 1, *World Ocean Atlas 2013*, NOAA Atlas NESDIS 73, 40 pp.
- Mertz, G., and D. G. Wright, 1992: Interpretations of JEBAR term. *J. Phys. Oceanogr.*, **22**, 301–305, doi:10.1175/1520-0485(1992)022<0301:IOTJT>2.0.CO;2.
- Qu, T., 2000: Upper-layer circulation in the South China Sea. *J. Phys. Oceanogr.*, **30**, 1450–1460, doi:10.1175/1520-0485(2000)030<1450:ULCITS>2.0.CO;2.
- , and Y. T. Song, 2009: Mindoro Strait and Sibutu Passage transports estimated from satellite data. *Geophys. Res. Lett.*, **36**, L09601, doi:10.1029/2009GL037314.
- , H. Mitsudera, and T. Yamagata, 2000: Intrusion of the North Pacific waters into the South China Sea. *J. Geophys. Res.*, **105**, 6415–6424, doi:10.1029/1999JC900323.
- , Y. Y. Kim, M. Yaremchuk, T. Tozuka, A. Ishida, and T. Yamagata, 2004: Can Luzon Strait transport play a role in conveying the impact of ENSO to the South China Sea? *J. Climate*, **17**, 3644–3657, doi:10.1175/1520-0442(2004)017<3644:CLSTPA>2.0.CO;2.
- Ray, R. D., 1998: Ocean self-attraction and loading in numerical tidal models. *Mar. Geod.*, **21**, 181–192, doi:10.1080/01490419809388134.
- Sasaki, H., M. Nonaka, Y. Masumoto, Y. Sasai, H. Uehara, and H. Sakuma, 2008: An eddy-resolving hindcast simulation of the quasiglobal ocean from 1950 to 2003 on the Earth Simulator. *High Resolution Numerical Modelling of the Atmosphere and Ocean*, K. Hamilton and W. Ohfuchi, Eds., Springer, 157–185.
- Shchepetkin, A. F., and J. C. McWilliams, 2005: The regional ocean modeling system: A split-explicit, free-surface, topography following coordinates ocean model. *Ocean Modell.*, **9**, 347–404, doi:10.1016/j.ocemod.2004.08.002.
- Su, J., 2004: Overview of the South China Sea circulation and its influence on the coastal physical oceanography outside the Pearl River Estuary. *Cont. Shelf Res.*, **24**, 1745–1760, doi:10.1016/j.csr.2004.06.005.
- Tian, J., Q. Yang, X. Liang, D. Hu, F. Wang, and T. Qu, 2006: The observation of Luzon Strait transport. *Geophys. Res. Lett.*, **33**, L19607, doi:10.1029/2006GL026272.
- Wang, G., S.-P. Xie, T. Qu, and R. X. Huang, 2011: Deep South China Sea circulation. *Geophys. Res. Lett.*, **38**, L05601, doi:10.1029/2010GL046626.
- Wyrtki, K., 1961: *Physical Oceanography of the Southeast Asian Waters*. NAGA Rep., Vol. 2, Scripps Institute of Oceanography, 195 pp.
- Xue, H., F. Chai, N. Pettigrew, D. Xu, M. Shi, and J. Xu, 2004: Kuroshio intrusion and the circulation in the South China Sea. *J. Geophys. Res.*, **109**, C02017, doi:10.1029/2002JC001724.
- Yuan, Y., G. Liao, and C. Yang, 2008: The Kuroshio near the Luzon Strait and circulation in the northern South China Sea during August and September 1994. *J. Oceanogr.*, **64**, 777–788, doi:10.1007/s10872-008-0065-6.
- Zhao, W., C. Zhou, J. Tian, Q. Yang, B. Wang, L. Xie, and T. Qu, 2014: Deep water circulation in the Luzon Strait. *J. Geophys. Res. Oceans*, **119**, 790–804, doi:10.1002/2013JC009587.
- Zweng, M. M., and Coauthors, 2013: *Salinity*. Vol. 2, *World Ocean Atlas 2013*, NOAA Atlas NESDIS 74, 39 pp.